Turbulence and multifractality in some models for active fluids

Rahul Pandit

Centre for Condensed Matter Theory, Department of Physics
Indian Institute of Science, Bangalore, India.

06 November 2023
Active Matter and Beyond, ICTS, Bangalore.

Felicitations

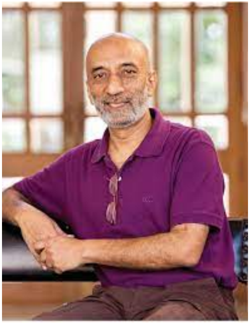

Sriram: Congratulations and best wishes!

Acknowledgements

John D Gibbon
Department of Mathematics
Imperial college, London

Nadia Bihari Padhan
Department of Physics
IISc, Bangalore

Kolluru Venkata Kiran
Department of Physics
IISc, Bangalore

Support: SERB, CSIR, UGC, NSM, and SERC (IISc).

References

- *Irreversibility in bacterial turbulence: Insights from the mean-bacterial-velocity model, Kolluru Venkata Kiran, Anupam Gupta, Akhilesh Kumar Verma, and Rahul Pandit,* **Phys. Rev. Fluids 8, 023102 (2023).**

- *Activity-induced droplet propulsion and multifractality, Nadia Bihari Padhan and Rahul Pandit,* **Physical Review Research, 5, L032013 (2023).**

- *Active-turbulence-induced coarsening arrest in the active Cahn-Hilliard-Navier-Stokes model, Nadia Bihari Padhan and Rahul Pandit, (Manuscript in preparation).*

- *An analytical and computational study of the incompressible Toner-Tu Equations, John D Gibbon, Kolluru Venkata Kiran, Nadia Bihari Padhan, and Rahul Pandit -* **Physica D: Nonlinear Phenomena, 2022**.

Outline

- Introduction to active fluids.
- Models for active fluids
- Illustrative results.
  - Irreversibiity in bacterial turbulence.
  - Active coarsening arrest and turbulence.
  - Self-propelled droplets.
  - Regularity criteria for the incompressible Toner-Tu equations.
- Conclusions.

Active Fluid Flows: Examples

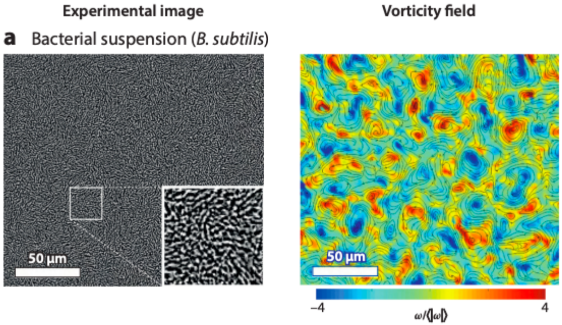

Annual Review of Condensed Matter Physics

Active Turbulence

Ricard Alert,[1,2] Jaume Casademunt,[3,4]
and Jean-François Joanny[5,6]

Confined Active Fluids: Examples

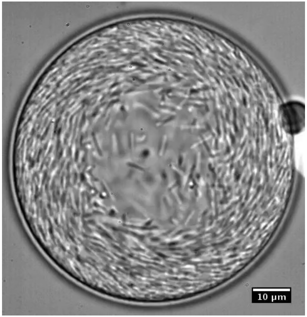

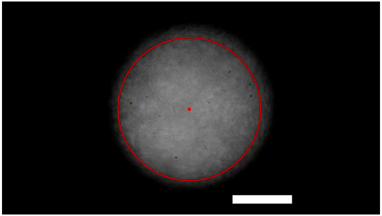

(left: Movie) A droplet of Bacillus subtilis (Formation of a single spiral vortex)
(right: Movie) Dense suspension of Escherichia coli inside a spherical droplet (Random walk)

(left): Confinement Stabilizes a Bacterial Suspension into a Spiral Vortex, R Goldstein et al., PRL, 2013.

(right): Bacteria driving droplets, Rodrigo Soto et al., Soft Matter, 2020

Direct Numerical Simulation (DNS)

To calculate the relevant fields:

- Simulation domain: periodic box of length 2π.
- N grid points in each direction.
- We solve the nonlinear equations by using a pseudospectral method (evaluate derivatives in Fourier space and products in physical space).
- We do not have to impose boundary conditions on a moving droplet boundary.
- Time marching: Semi-implicit exponential time differencing with RK2 method (ETD2RK).
- Computers with Graphics Processing Units (e.g., the NVIDIA A100, V100), which we program in CUDA.
- Massively Parallel pseudospectral FORTRAN and C codes.

Irreversiblity in Bacterial Turbulence

PHYSICAL REVIEW FLUIDS **8**, 023102 (2023)

Irreversibility in bacterial turbulence: Insights from the mean-bacterial-velocity model

Kolluru Venkata Kiran,[1,*] Anupam Gupta,[2,†] Akhilesh Kumar Verma,[3,‡] and Rahul Pandit[1,§]

[1]*Centre for Condensed Matter Theory, Department of Physics, Indian Institute of Science, Bangalore 560012, India*

[2]*Department of Physics, Indian Institute of Technology (IIT) Hyderabad, Kandi, Sangareddy, Telangana 502285, India*

[3]*Mathematics Institute, Zeeman Building, University of Warwick, Coventry CV4 7AL, United Kingdom*

Mean-Bacterial-Velocity Model

- Mean-bacterial-velocity model [H.H. Wensink, *et al.*, PNAS, 109, 14308 (2012)]or the Toner-Tu-Swift-Hohenberg (TTSH) model [Alert *et al.*, *op. cit.*] for the velocity field $\mathbf{u}(\mathbf{x}, t)$.
- This model has been employed to study turbulence in dense suspensions of *Bacilis subtilis*:

$$\begin{aligned}\frac{\partial \mathbf{u}}{\partial t} + \lambda_0 \mathbf{u}.\nabla \mathbf{u} &= -\nabla P - (\alpha + \beta |\mathbf{u}|^2)\mathbf{u} \\ &+ \Gamma_0 \nabla^2 \mathbf{u} - \Gamma_2 \nabla^4 \mathbf{u}; \\ \nabla \cdot \mathbf{u} &= 0. \end{aligned} \tag{1}$$

- $P(\mathbf{x}, t)$: pressure; the constant density $\rho = 1$.
- This equation is not Galilean invariant; it reduces to the Navier-Stokes equation with friction for $\Gamma_0 > 0, \alpha > 0, \Gamma_2 = 0, \lambda_0 = 1$, and $\beta = 0$.

Mean-Bacterial-Velocity Model

- We use periodic boundary conditions because we study statistically homogeneous and isotropic bacterial turbulence.
- We restrict ourselves to two dimensions (2D) as most experiments in this field have been conducted in quasi-2D systems.
- $\Gamma_0 < 0$ and $\Gamma_2 < 0$; a spatial Fourier transform of the equation, followed by a linear-stability analysis about the spatially uniform state, yields the wave vectors $\mathbf{k}$, with magnitude k, for which there are linearly unstable modes.
- Characteristic length, velocity, and time scales:

$$\Lambda = 2\pi\sqrt{\frac{2\Gamma_2}{\Gamma_0}};\ v_0 = \sqrt{\frac{|\Gamma_0|^3}{\Gamma_2}};\ \theta = \frac{\Lambda}{v_0}. \tag{2}$$

- These unstable modes inject energy into the system.
- This energy is dissipated by (a) the linearly stable modes, (b) the cubic term with the coefficient $\beta > 0$, and (c) the linear term with the coefficient α, if $\alpha > 0$.

Mean-Bacterial-Velocity Model

- Moreover, there is energy injection, or *activity*, if $\alpha < 0$.
- $\Gamma_0 < 0$ and $\lambda_0 \neq 1$ also induce activity.
- $\lambda_0 > 1$ for *pusher swimmers* like *B. subtilis*.
- We hold λ_0, β, and Γ_0 fixed, and we tune the activity principally by varying α.
- The interplay between these energy-injection and dissipation terms leads to self-sustained, turbulence-type patterns. The effective viscosity
$$k^2\nu_{eff}(k) = \left(\alpha + 2\beta u_{rms}^2 + \Gamma_0 k^2 + \Gamma_2 k^4\right) \tag{3}$$
can be used to rewrite Eq. (1) in a Navier-Stokes form.
- Clearly, the wave numbers k at which energy is injected (dissipated) are those with $\nu_{eff}(k) < 0$ (> 0); the root-mean-square velocity u_{rms} must be obtained from a calculation.
- We solve this equation by a pseudospectral direct numerical simulation (DNS) with $N^2 = 1024^2$ collocation points (for parameters see K.V. Kiran *op. cit.*); we have checked in representative cases that our results are unchanged if we use $N^2 = 2048^2$ collocation points.

Vorticity and Energy Spectra

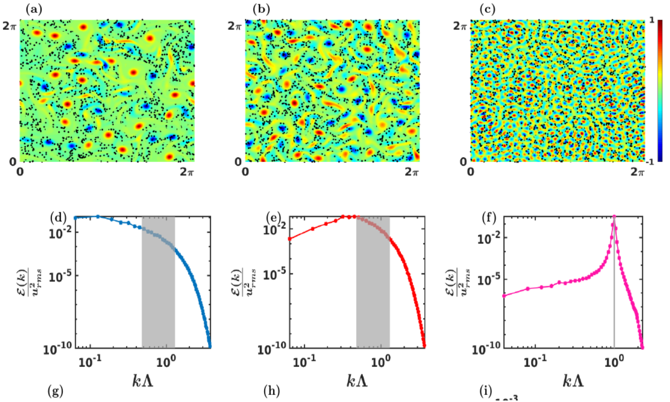

Filled contour plots of the vorticity, with some tracers (black points), and energy spectrta for illustrative values of α.; the gray-shaded areas indicate the ranges of k for which $\nu_{eff}(k) < 0$.

Flux and Scales

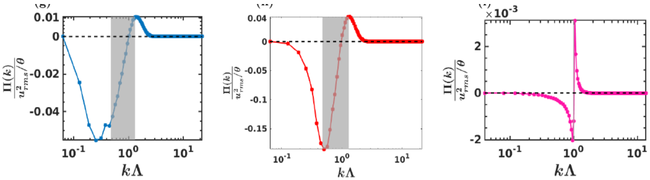

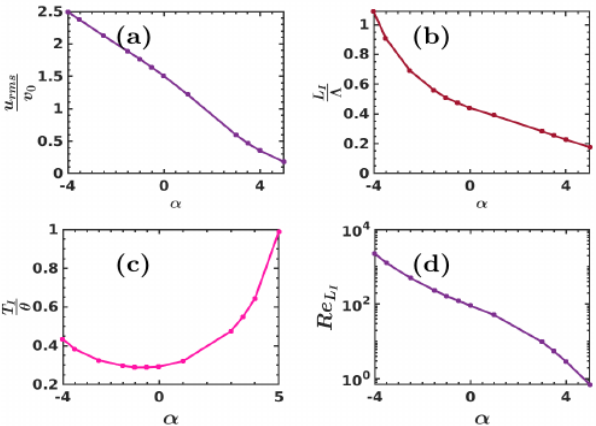

Irreversibility: Fluid Turbulence

- Irreversibility: not easily apparent if we look at movies, played forward or backward in time, of Lagrangian or inertial particles that are advected by turbulent flows.
- However, the statistics of such particles in turbulent flows yields signatures of this irreversibility [see, e.g., H. Xu, *et al.* Flight–crash events in turbulence, PNAS111, 7558 (2014); and A. Bhatnagar, *et al.*, Heavy inertial particles in turbulent flows gain energy slowly but lose it rapidly, Phys. Rev. E 97, 033102 (2018)].
- We analyse (a) the increments

  $$W(t, \tau) \equiv E(t + \tau) - E(t) \tag{4}$$

  of the particle energy E at time t or (b) the power

  $$p_L(t) \equiv \frac{dE}{dt} = a_L v_L, \tag{5}$$

  with v_L the magnitude of the tracer velocity and a_L the component of its acceleration along its trajectory.
- It has been found that probability distribution functions (PDFs) of W and p_L, i obtained by averaging over t and the trajectories of all tracers, are negatively skewed, i.e., on average, such particles *lose energy faster than they gain it.*

Irreversibility: Bacterial Turbulence

- We characterise irreversibility in *bacterial turbulence* in the mean-bacterial-velocity model..
- We uncover an important, qualitative way in which irreversibility in bacterial turbulence is different from its fluid-turbulence counterpart:
- For large positive (or large but negative) values of the *friction* (or *activity*) parameter α, the PDFs of $W(\tau)$ or p_L are *positively* skewed. We quantify this asymmetry by computing the skewnesses:

$$\mathcal{P}_{Sk} = \frac{\langle p_L^3 \rangle}{\langle p_L^2 \rangle^{\frac{3}{2}}} \text{ and } \mathcal{W}_{Sk}(\tau) = \frac{\langle W^3(\tau) \rangle}{\langle W^2(\tau) \rangle^{\frac{3}{2}}}. \quad (6)$$

- Thus, irreversibility in bacterial turbulence can lead, on average, to *particles gaining energy faster than they lose it*, for certain ranges of values of α.

Energy and Skewness

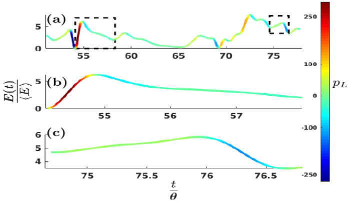

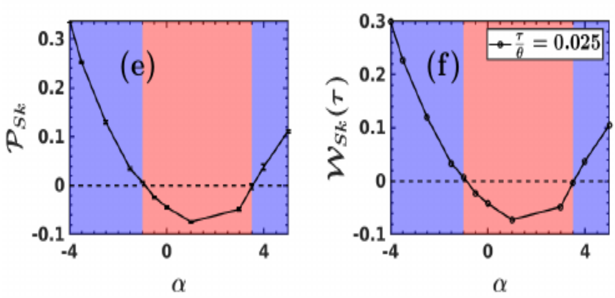

Top panel: Energy vs time. Bottom panel: (e) the skewness $\mathcal{P}_{Sk}$ and (f) $\mathcal{W}_{Sk}(\tau)$ for $\tau/\theta = 0.025$; blue and pink shading indicate, respectively, ranges of α in which the skewnesses are positive and negative.

Probability Distribution Functions (PDFs)

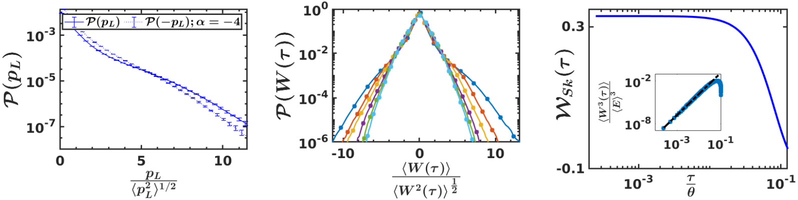

(a) Semi-log plot of the normalized PDFs (a) $\mathcal{P}(p_L)$ and (b) $\mathcal{P}(W(\tau))$, with τ/θ going from $0.025, 0.08, 0.13, 0.25, 0.38$, to 0.50, as we move from the outermost to the innermost curve; in (a) negative values of p_L (dashed) are reflected about the vertical axis to highlight the asymmetry of $\mathcal{P}(p_L)$. (c) Log-Log (base 10) plot versus τ/θ of the skewness $\mathcal{W}_{Sk}(\tau)$. Inset: for the same range of τ/θ, a log-log plot versus τ/θ of $\langle W^3(\tau)\rangle/\langle E\rangle^3$; the dashed black line is a fit to $\langle W^3(\tau)\rangle/\langle E\rangle^3 \sim (\tau/\theta)^3$.

Probability Distribution Functions (PDFs)

Okubo-Weiss parameter: $Q_L(t) = \left.\frac{\omega^2 - \sigma^2}{4}\right|_{x_L(t)}$:

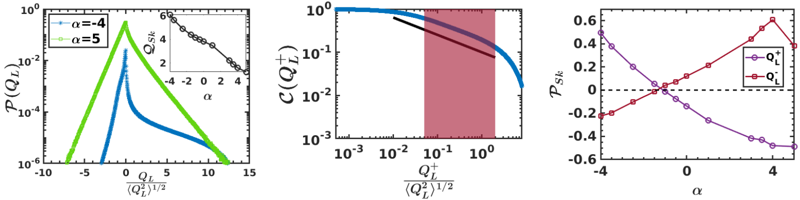

(a) Semi-log plots of $\mathcal{P}(Q_L)$ for runs A1 (blue) and A13 (green). Inset gives the plot versus α of skewness, $\mathcal{Q}_{Sk}$, for $\mathcal{P}(Q_L)$. (b) Log-log plot of $\mathcal{C}(Q_L^+)$ for run A1; the shaded region shows a power-law and the solid black line gives the fit $\mathcal{C}(Q_L^+) \sim [Q_L^+]^{-\vartheta}$, with $\vartheta = 0.37 \pm 0.04$. (c) Plots versus α of $\mathcal{P}_{Sk}$ for the conditioned PDFs (see text) $\mathcal{P}(p_L|Q_L^+)$ (violet) and $\mathcal{P}(p_L|Q_L^-)$ (maroon).

Conclusions I

- We have shown how to use the mean-bacterial-flow model to study irreversibility of bacterial turbulence.
- Quasi-2D experiments on dense suspension of aerobic bacteria, e.g., *B. subtilis*, show that the average speed of bacterial flow increases with the oxygen concentration.
- We can increase the activity by making α large and negative; in experiments, the activity can be increased by enhancing the oxygen, because the polar-ordered velocity scale $v_p = \sqrt{\frac{|\alpha|}{\beta}}$ is a measure of the swimming speed of bacteria; $u_{rms} \propto \alpha$ (cf. C. P. Sanjay and A. Joy, Phys. Rev. Fluids 5, 024302 (2020)).
- In the frictional or $\alpha > 0$ regime, the value of α can be tuned in experiments by changing the bottom friction or the air-drag-induced friction.
- Therefore, experiments on dense bacterial suspensions should be able to examine irreversibility in bacterial turbulence as a function of the activity as we have done above.

Active coarsening arrest and turbulence

Active-turbulence-induced coarsening arrest in the active Cahn-Hilliard-Navier-Stokes model

Nadia Bihari Padhan,[1,*] Kolluru Venkata Kiran,[1,†] and Rahul Pandit[1,‡]

[1] *Centre for Condensed Matter Theory, Department of Physics, Indian Institute of Science, Bangalore, 560012, India.*

Active coarsening arrest and turbulence

- Motivation: To study the active coarsening arrest and turbulence in active model H in the presence of inertia.
- The model studies the motility-induced phase separation (MIPS) in the presence of hydrodynamic interactions.

- Order parameter: $\psi \rightarrow$ active microswimmers field.

$$\mathcal{F}[\psi, \nabla\psi]/\Omega = \frac{3}{16}\frac{\sigma}{\epsilon}(\psi^2 - 1)^2 + \frac{3}{4}\sigma\epsilon|\nabla\psi|^2$$

- $\psi \simeq +1 \rightarrow$ High density; $\psi \simeq -1 \rightarrow$ Low density

Active Model H: Scalar Active Matter in a Momentum-Conserving Fluid, A. Tiribocchi, R. Wittkowski, D, Marenduzzo, and M.E. Cates, Phys. Rev. Lett. **115**, *188302 (2015).*

Active CHNS model

$$
\begin{aligned}
\partial_t\psi + (\boldsymbol{u}\cdot\nabla)\psi &= M\nabla^2\left(\frac{\delta\mathcal{F}}{\delta\psi}\right)\\
\partial_t\omega + (\boldsymbol{u}\cdot\nabla)\omega &= \nu\nabla^2\omega - \alpha\omega + [\nabla\times\mathfrak{S}^{\psi}]\\
\nabla\cdot\boldsymbol{u} &= 0 \quad \omega = (\nabla\times\boldsymbol{u})\\
\mathfrak{S}^{\psi} &= -(3/2)\zeta\epsilon\nabla^2\psi\nabla\psi
\end{aligned}
$$

- Important: $\sigma \neq \zeta$
  $\zeta > 0 \rightarrow$ Extensile swimmers $\zeta < 0 \rightarrow$ Contractile swimmers
- We consider $\zeta < 0$ to study turbulence.

Active Model H: Scalar Active Matter in a Momentum-Conserving Fluid, A. Tiribocchi, et al., op. cit.

Active coarsening arrest

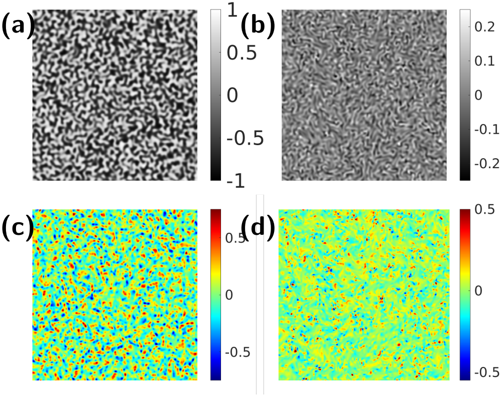

Figure: Pseudo-gray-scale plots of the ψ field [at representative times in the nonequilibrium statistically steady state (NESS)] for the activity parameter (a) $|\zeta| = 0.01$ and (b) $|\zeta| = 1.5$. Pseudocolor plots of the vorticity field, normalized by the maximum of $|\omega|$, are shown in (c) and (d) for the parameters in (a) and (b), respectively.

Active coarsening arrest

- Coarsening length scale, $\mathcal{L}(t) = \frac{\sum_k \Lambda(k,t)}{\sum_k \Lambda(k,t)}$
- $\Lambda(k,t) \equiv \sum_{k \le k' < k+1} |\hat{\psi}(\boldsymbol{k}', t)|^2$

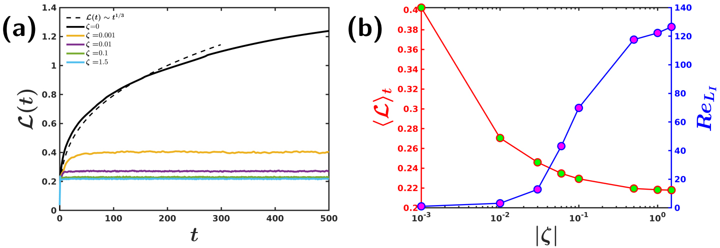

Figure: (a) Plot of $\mathcal{L}(t)$ versus time t for various values of $|\zeta|$; the plot for $\zeta = 0$ shows growth that is consistent with the **Lifshitz-Slyozov** form $\boldsymbol{\mathcal{L}(t) \sim t^{1/3}}$ (dashed line); $\mathcal{L}(t)$ saturates to a finite value for $|\zeta| > 0$. (b) Log-linear plots of the mean coarsening-arrest scale $L_c = \langle \mathcal{L}(t) \rangle_t$ (red curve) and the integral-scale Reynolds number Re_{L_I} (blue curve) versus $|\zeta|$.

Active CHNS: Spectra and Budget

- Energy spectrum: $\mathcal{E}(k)$
- Inertial energy transfer $[T(k)]$, the energy dissipations arising from the friction $[D_\alpha(k)]$ and the viscosity $[D_\nu(k)]$, and the energy transfer via the active stress $[S^\Phi(k)]$.

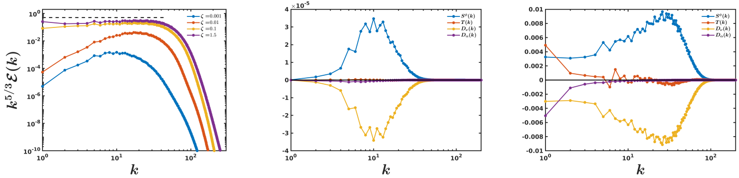

Figure: Left panel: Log-log plot of $\mathcal{E}(k)$ versus k. Energy budget for low (middle panel) and high (right panel) $|\zeta|$.

Conclusions II

- We have shown that active turbulence arrests phase separation [cf., its fluid-turbulence counterpart in P. Perlekar, N. Pal, and R. Pandit, Scientific Reports 7, 44589 (2017) and references therein].
- We quantify this suppression by showing how the coarsening-arrest length $\mathcal{L}(t)$.
- We characterise the statistical properties of this active-scalar turbulence by employing spectra and fluxes that are used in fluid turbulence and domain growth.
- Our results are of potential relevance to systems of contractile swimmers, e.g., *Chlamydomonas reinhardtii* and synthetic active colloids.

Self-propelled Droplets

PHYSICAL REVIEW RESEARCH **5**, L032013 (2023)

Letter

Activity-induced droplet propulsion and multifractality

Nadia Bihari Padhan * and Rahul Pandit †

Centre for Condensed Matter Theory, Department of Physics, Indian Institute of Science, Bangalore 560012, India

Self-propelled Droplets

- Motivation: Self-organization of microswimmers (extensile and contractile) confined to a droplet.
- Two order parameters: $\phi \rightarrow$ binary emulsion droplet;
  $\psi \rightarrow$ active microswimmers field.

$$\mathcal{F}[\phi, \nabla\phi, \psi, \nabla\psi]/\Omega = \frac{3}{16}\left(\frac{\sigma_1}{\epsilon_1}(\phi^2-1)^2 + \frac{\sigma_2}{\epsilon_2}(\psi^2-1)^2\right) - \beta\phi\psi$$
$$+\frac{3}{4}\left(\sigma_1\epsilon_1|\nabla\phi|^2 + \sigma_2\epsilon_2|\nabla\psi|^2\right)$$

- $\phi \simeq +1 \rightarrow$ Fluid-A; $\phi \simeq -1 \rightarrow$ Fluid-B.
- $\psi \simeq +1 \rightarrow$ High density; $\psi \simeq -1 \rightarrow$ Low density
- $\beta > 0 \rightarrow$ Attractive coupling.

Self-propelled droplet: Active CHNS model

$$
\begin{aligned}
\partial_t \phi + (\boldsymbol{u} \cdot \nabla)\phi &= M_1 \nabla^2 \left(\frac{\delta \mathcal{F}}{\delta \phi} \right) \\
\partial_t \psi + (\boldsymbol{u} \cdot \nabla)\psi &= M_2 \nabla^2 \left(\frac{\delta \mathcal{F}}{\delta \psi} \right) \\
\partial_t \omega + (\boldsymbol{u} \cdot \nabla)\omega &= \nu \nabla^2 \omega - \alpha \omega + [\nabla \times (\mathfrak{S}^{\phi} + \mathfrak{S}^{\psi})] \\
\nabla \cdot \boldsymbol{u} &= 0 \quad \omega = (\nabla \times \boldsymbol{u}) \\
\mathfrak{S}^{\phi} &= -(3/2)\sigma_1 \epsilon_1 \nabla^2 \phi \nabla \phi \\
\mathfrak{S}^{\psi} &= -(3/2)\tilde{\sigma}_2 \epsilon_2 \nabla^2 \psi \nabla \psi
\end{aligned}
$$

- Important: $\sigma_2 \neq \tilde{\sigma}_2$
  $\tilde{\sigma}_2 > 0 \rightarrow$ Extensile swimmers
  $\tilde{\sigma}_2 < 0 \rightarrow$ Contractile swimmers
- Activity parameter: $A = \tilde{\sigma}_2 / \sigma_2$

Self-propelled droplet: Dynamics for different A

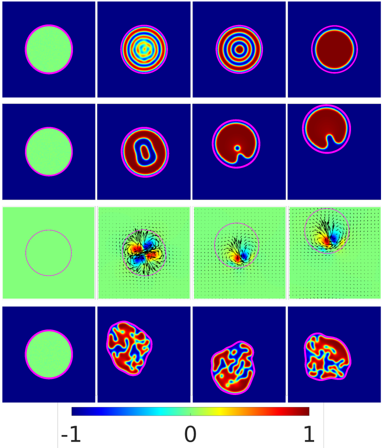

Figure: Illustrative pseudocolor plots of ψ, with the $\phi = 0$ contour shown in magenta, at different representative times (increasing from left to right) for (a) $A = 0$ (**no droplet propulsion**), (b) $A = 0.15$ (**rectilinear droplet propulsion**), and (d) $A = 1$ (**turbulent droplet propulsion**). In (c) we show, for $A = 0.15$, vector plots of the velocity field $\boldsymbol{u}$, with the $\phi = 0$ contour line (magenta), overlaid on a pseudocolor plot of the vorticity ω normalised by its maximal value; the lengths of velocity vectors are proportional to their magnitudes.

Self-propelled droplets: Animations

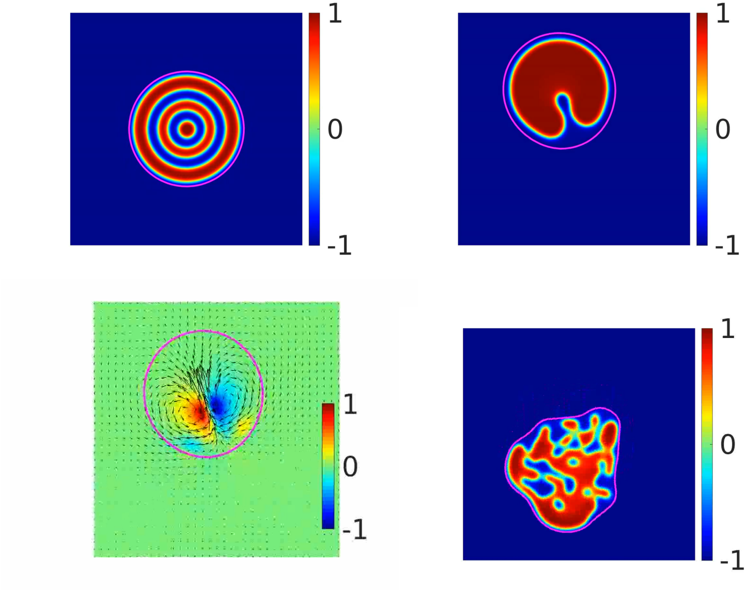

Self-propelled droplet: MSD

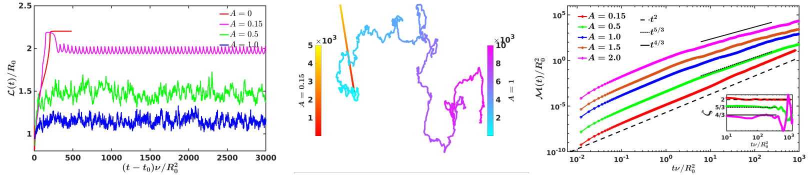

(a) Plots of the integral length scale $\mathcal{L}(t)/R_0$ versus $(t-t_0)\nu/R_0^2$ for $A=0$ (red curve), $A=0.15$ (magenta curve), $A=0.5$ (green curve), and and $A=1$ (blue curve), with t_0 is a non-universal offset that depends on A. (b) Illustrative trajectories of the droplet's CM for $A=0.15$ (orange) and $A=1$ (blue-purple), with colorbars indicating the simulation time. (c) Log-log plots of the mean-square-displacement $\mathcal{M}(t)$ versus $t\nu/R_0^2$ (after the removal of initial transients) for droplet-CM trajectories: $A=0.15$ (red), $A=0.5$ (green), $A=1$ (blue), $A=1.5$ (dark orange), and $A=2$ (magenta); initially these plots show ballistic regimes, but, at large times, we see $\mathcal{M}(t)\sim t^{\zeta}$, with $\zeta=2$ (rectilinear motion for $A=0.15$), and superdiffusive regimes with $\zeta=1.67\pm0.02\simeq 5/3$ (for $A=0.5$) and $\zeta=1.28\pm0.05\simeq 4/3$ (for $A=2$) via local-slope analysis (the inset shows plots of ζ versus t); plots for different values of A are displaced vertically for ease of visualization.

Multifractal interface fluctuations

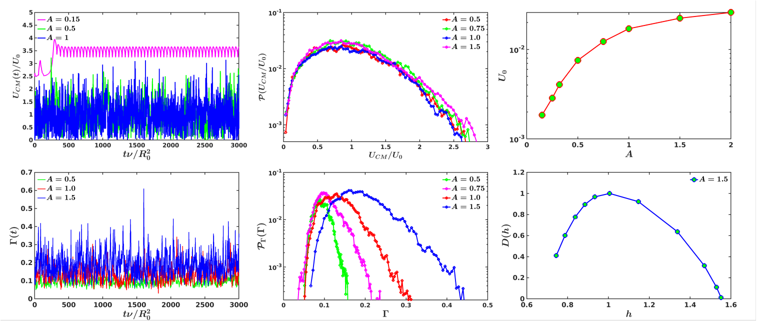

Figure: (a) Plots versus the non-dimensionalized time $t\nu/R_0^2$ of the scaled droplet-CM speed U_{CM}/U_0 for $A = 0.15$ (magenta curve, which has been moved up to aid visualization), $A = 0.5$ (green) and $A = 1$ (blue). (b) Semilog plots of the PDF $\mathcal{P}(U_{CM}/U_0)$ for $A = 0.5$ (red), $A = 0.75$ (green), $A = 1$ (blue), and $A = 1.5$ (magenta). (c) Semilog plot of U_0 versus A. (d) Plots versus $t\nu/R_0^2$ of the normalised droplet perimeter $\Gamma(t)$ for $A = 0.5$ (green), $A = 1$ (red), and $A = 1.5$ (blue). (e) Semilog plots of the PDF of $\mathcal{P}_\Gamma(\Gamma)$ for $A = 0.5$ (green), $A = 0.75$ (magenta), $A = 1$ (red), and $A = 1.5$ (blue). (f) Plots of the multifractal $D(h)$ versus the Hurst exponent h, obtained from $\Gamma(t)$, for $A = 1.5$.

Conclusions III

- We have developed a minimal model for assemblies of contractile swimmers, without alignment interactions, en- capsulated in a droplet of a binary-fluid emulsion.
- Our model captures the droplet interface (via the $\phi = 0$ contour) and its multifractal fluctuations.
- Our model also leads to droplet self-propulsion, which is rectilinear at low $A(\simeq 0.15)$ and chaotic for large values of A, at which the CM of the droplet shows superdiffusive motion.
- Our results are of potential relevance to systems of contractile swimmers, e.g., *Chlamydomonas reinhardtii*.

Incompressible Toner-Tu (ITT) Model

Physica D 444 (2023) 133594

Contents lists available at ScienceDirect

Physica D

journal homepage: www.elsevier.com/locate/physd

An analytical and computational study of the incompressible Toner–Tu Equations

John D. Gibbon [a], Kolluru Venkata Kiran [b], Nadia Bihari Padhan [b], Rahul Pandit [b,*]

[a] *Department of Mathematics, Imperial College London, London SW7 2AZ, UK*
[b] *Centre for Condensed Matter Theory, Department of Physics, Indian Institute of Science, Bangalore, 560012, India*

Incompressible Toner-Tu (ITT) Model

$$(\partial_t + \lambda \boldsymbol{u} \cdot \nabla)\, \boldsymbol{u} + \nabla p = \alpha \boldsymbol{u} + \nu \Delta \boldsymbol{u} - \beta\, \boldsymbol{u} |\boldsymbol{u}|^2 \,. \tag{7}$$

Introduce a typical velocity field U_0 for which we have two definitions:

$$U_0 = \sqrt{\alpha/\beta}\,; \qquad\qquad U_0 = \nu/L\,. \tag{8}$$

Then primed dimensionless variables are defined thus :

$$\begin{aligned} \boldsymbol{x}' &= L^{-1}\boldsymbol{x}\,; \qquad t' = U_0 L^{-1} t\,; \\ \boldsymbol{u}' &= \lambda U_0^{-1} \boldsymbol{u}\,; \qquad p' = \lambda U_0^{-2} p\,. \end{aligned} \tag{9}$$

Non-Dimensional ITT

With the primed variables defined as above, we have the following dimensionless form for ITT:

$$(\partial_t + \boldsymbol{u} \cdot \nabla)\, \boldsymbol{u} + \nabla p \quad = \quad \alpha_0 \boldsymbol{u} + \mathrm{Re}_\nu^{-1} \Delta \boldsymbol{u} - \mathrm{Re}_\beta \, \boldsymbol{u} |\boldsymbol{u}|^2, \tag{10}$$

,together with the incompressibility condition div $\boldsymbol{u} = 0$. These operate on the unit periodic box $V_d = [0, 1]^d$. The non-dimensional parameters are defined as follows :

$$\mathrm{Re}_\nu \quad = \quad \frac{U_0 L}{\nu}, \qquad \mathrm{Re}_\beta = \frac{\beta\, U_0 L}{\lambda^2}, \qquad \alpha_0 = L \alpha U_0^{-1}. \tag{11}$$

An invariant scaling for ITT and NSE

The incompressible NSEs and the ITT equations possess the following powerful invariant scaling property involving an arbitrary parameter ℓ:

$$\boldsymbol{x}' = \ell^{-1}x; \quad t' = \ell^{-2}t; \quad \boldsymbol{u} = \ell^{-1}\boldsymbol{u}'; \tag{12}$$

which means that these equations are valid at every scale. The effect of this invariance is to scale the norms $\|\nabla^n \boldsymbol{u}\|_{2m}$ defined by

$$\|\nabla^n \boldsymbol{u}\|_{2m} = \left(\int_{V_d} |\nabla^n \boldsymbol{u}|^{2m} dV_d\right)^{1/2m} \tag{13}$$

in the following way:

$$\|\nabla^n \boldsymbol{u}\|_{2m} = \ell^{-1/\alpha_{m,n,d}} \|\nabla'^n \boldsymbol{u}'\|_{2m}; \; \alpha_{n,m,d} = \frac{2m}{2m(n+1)-d}. \tag{14}$$

An invariant scaling for ITT and NSE

The $\alpha_{n,m,d}$ are a product of the invariance property (12). A dimensionless version of the norms defined in (14) is given by

$$F_{n,m,d} := \nu^{-1} L^{1/\alpha_{n,m,d}} \|\nabla^n \boldsymbol{u}\|_{2m} . \tag{15}$$

It has been shown that, for $d = 2$, 3, and for $n \geq 1$ and $1 \leq m \leq \infty$, weak solutions of the incompressible NSEs obey

$$\left\langle F_{n,m,d}^{(4-d)\alpha_{n,m,d}} \right\rangle_T < \infty . \tag{16}$$

The angular brackets $\langle \cdot \rangle_T$ represent the time average up to a time T, i.e.,

$$\langle \cdot \rangle_T = \frac{1}{T} \int_0^T \cdot \, d\tau . \tag{17}$$

An invariant scaling for ITT and NSE

The parallel scaling properties of the ITT equations and the NSEs suggest that the exponents $\alpha_{n,m,d}$ in (14) should be the same in both cases. Therefore, taking into account the factor of $4-d$ in the exponent, we define the following for ITT :

- d=2
$$P_{n,m} = \|\nabla^n \boldsymbol{u}\|_{2m}^{2\alpha_{n,m,2}}; \qquad \alpha_{n,m,2} = \frac{m}{m(n+1)-1}. \tag{18}$$
- d=3
$$Q_{n,m} = \|\nabla^n \boldsymbol{u}\|_{2m}^{\alpha_{n,m,3}}; \qquad \alpha_{n,m,3} = \frac{2m}{2m(n+1)-3}. \tag{19}$$

Weak solutions for ITT, d=2

We prove analytically the following inequalities for d=2:

- With the definition $\langle P_{0,m}\rangle_T = \left\langle \|\boldsymbol{u}\|_{2m}^{\frac{2m}{m-1}} \right\rangle_T$, for $m > 2$,

$$\langle P_{0,m}\rangle_T \le c\,\mathcal{A}_0^{\frac{m}{m-1}}\,(\alpha_0 \mathrm{Re}_\nu)^{\frac{m-2}{m-1}}\,. \tag{20}$$

- $n = 1$ and $m = 1$

$$\langle P_{1,1}\rangle_T \le \alpha_0 \mathcal{A}_0 \mathrm{Re}_\nu\,, \tag{21}$$

- $n = 1$

$$\langle P_{1,m}\rangle_T \quad \le \quad c_m\,(\alpha_0 \mathrm{Re}_\nu)^{\frac{3m-2}{2m-1}}\,\mathcal{A}_0^{\frac{m}{2m-1}}\,. \tag{22}$$

- $n \ge 2$,

$$\langle P_{n,m}\rangle_T \le c_{n,m}\alpha_0^{\frac{2m}{m(n+1)-1}}\left(\alpha_0 \mathcal{A}_0 \mathrm{Re}_\nu^3\right)^{\frac{mn-1}{m(n+1)-1}}\,. \tag{23}$$

In all the above inequalities, $c_{n,m}$ are constants and $\mathcal{A}_0 \equiv \alpha_0 \mathrm{Re}_\beta^{-1}$

Computational results, d=2

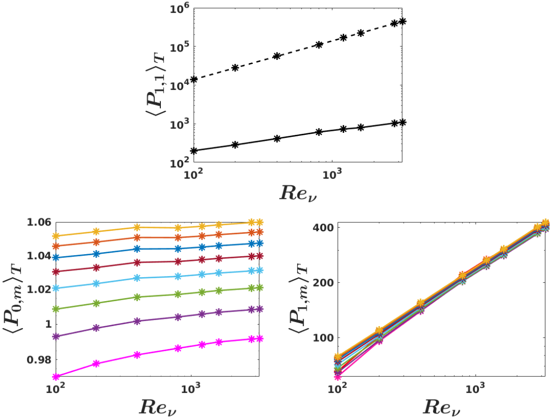

Figure: Illustrative plots for $U_0 = \sqrt{\alpha/\beta}$ for various runs in d=2. First row: plots versus Re_ν of $\langle P_{1,1}\rangle_T$ (solid black line). Second row: Plots versus Re_ν of $\langle P_{0,m}\rangle_T$ and $\langle P_{1,m}\rangle_T$. Curves for $m = 2, 3, 4, 5, 6, 7, 8, 9,$ and 10 are drawn in red, pink; violet, green, cyan, maroon, blue, orange, and yellow, respectively. Dashed blacked lines gives us the analytical upper bound.

Global regularity of ITT for d=2

Defining n derivatives of $\boldsymbol{u}$ in $L^2(V_d)$ as

$$H_n = \int_{V_d} |\nabla^n \boldsymbol{u}|^2 dV_d \,. \tag{24}$$

We can first establish a full ladder theorem:

$$\begin{aligned} \tfrac{1}{2}\dot{H}_n &\leq \alpha_0 H_n - \mathrm{Re}_\nu^{-1} H_{n+1} + c_{n,1} H_{n+1}^{1/2} H_n^{1/2} \|\boldsymbol{u}\|_\infty \\ &+ c_{n,2}\mathrm{Re}_\beta H_n \|\boldsymbol{u}\|_\infty^2 \,; \end{aligned} \tag{25}$$

and subsequently show:

$$\begin{aligned} H_1(T) &\leq H_1(0)\exp\left\{\int_0^T \left(\alpha_0 + c\,\mathrm{Re}_\beta^2 \mathrm{Re}_\nu \|\boldsymbol{u}\|_4^4\right)\, d\tau\right\} \\ &\leq H_1(0)\exp\left\{\alpha_0\left(1 + c\,\mathrm{Re}_\beta^2\mathrm{Re}_\nu \mathcal{A}_0^2\right)\, T\right\}\,, \end{aligned} \tag{26}$$

which is finite for every finite T. Control over the H_1-norm establishes global regularity in this $2d$ case but not a global attractor, which requires a uniform bound for all t.

Weak solutions for ITT, d=3

We prove analytically the following inequalities for d=3:

- With the definition $Q_{0,m} = |\boldsymbol{u}|_{2m}^{\frac{2m}{2m-3}}$, for $m > 2$,

$$\langle Q_{0,m} \rangle_T \leq c\, \mathcal{A}_0^{\frac{2(m+3)}{5(2m-3)}} \left(\alpha_0 \mathrm{Re}_\nu^2\right)^{\frac{9(m-2)}{5(2m-3)}} . \tag{27}$$

- For $m = 1$ and $n = 1$ and $n = 1$

$$\langle Q_{1,1} \rangle_T \leq \alpha_0 \mathcal{A}_0 \mathrm{Re}_\nu ; \langle Q_{2,1} \rangle_T \leq c\, \alpha_0 \mathrm{Re}_\nu^2 . \tag{28}$$

- For $n \geq 2$ and $m \geq 1$,

$$\langle Q_{n,m} \rangle_T < \infty \tag{29}$$

Computational results, d=3

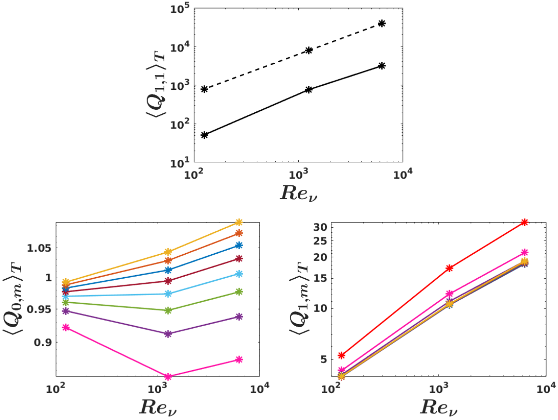

Figure: Illustrative plots for $U_0 = \sqrt{\alpha/\beta}$ for various runs in d=3. First row: plots versus Re_ν of $\langle Q_{1,1} \rangle_T$ (solid black line). Second row: Plots versus Re_ν of $\langle Q_{0,m} \rangle_T$ and $\langle Q_{1,m} \rangle_T$. Curves for $m = 2, 3, 4, 5, 6, 7, 8, 9,$ and 10 are drawn in red, pink; violet, green, cyan, maroon, blue, orange, and yellow, respectively. Dashed blacked lines gives us the analytical upper bound.

Conclusions IV

- The incompressible Toner–Tu (ITT) partial differential equations (PDEs) are an important example of a set of active-fluid PDEs. They share certain properties with the Navier–Stokes equations (NSEs), such as the same scaling invariance, but there are also important differences.
- The ITT equations have no additive forcing; instead, they include a linear, activity term $\alpha \boldsymbol{u}$ which pumps energy into the system, but also a negative $\propto \boldsymbol{u}|\boldsymbol{u}|2$ that provides a platform for either frozen or statistically steady states.
- In the $d = 2$ ITT, we have not only established global regularity of solutions, but we have also shown the existence of bounded hierarchies of weighted, time-averaged norms of both higher derivatives and higher moments of the velocity field.
- We have obtained similar bounded hierarchies for Leray-type weak solutions for the $d = 3$ ITT.
- We have presented results for these norms from our $d = 2$ and $d = 3$ DNSs and contrasted them with their Navier–Stokes counterparts.

Thank you for your attention.